Raindrop Size Distribution in Different Climatic Regimes from Disdrometer and Dual-Polarized Radar Analysis

V. N. Bringi, V. Chandrasekar, and J. Hubbert

Colorado State University, Fort Collins, Colorado

E. Gorgucci

Instituto di Fisica dell'Atmosfera (CNR), Rome, Italy

W. L. Randeu and M. Schoenhuber

Technical University of Graz and Joanneum Research, Graz, Austria

ABSTRACT

The application of polarimetric radar data to the retrieval of raindrop size distribution parameters and rain rate in samples of convective and stratiform rain types is presented. Data from the Colorado State University (CSU), CHILL, NCAR S-band polarimetric (S-Pol), and NASA Kwajalein radars are analyzed for the statistics and functional relation of these parameters with rain rate. Surface drop size distribution measurements using two different disdrometers (2D video and RD-69) from a number of climatic regimes are analyzed and compared with the radar retrievals in a statistical and functional approach. The composite statistics based on disdrometer and radar retrievals suggest that, on average, the two parameters (generalized intercept and median volume diameter) for stratiform rain distributions lie on a straight line with negative slope, which appears to be consistent with variations in the microphysics of stratiform precipitation (melting of larger, dry snow particles versus smaller, rimed ice particles). In convective rain, ''maritime-like'' and ''continental-like'' clusters could be identified in the same two-parameter space that are consistent with the different multiplicative coefficients in the $Z = aR^{1.5}$ relations quoted in the literature for maritime and continental regimes.

1. Introduction

Since the early articles by Seliga and Bringi (1976, 1978), a long-standing goal in radar polarimetric research has been the retrieval of the raindrop size distribution using measurements of reflectivity (Z_h), differential reflectivity (Z_{dr}), and specific differential phase (K_{dp}). The drop size distribution (DSD) is known to vary both spatially and temporally not only within a specific storm type but also across differing storm types and climatic regimes. The DSD can be characterized by three parameters such as characteristic diameter, concentration, and DSD shape, and analytic forms such as the gamma or lognormal distributions have been widely used (e.g., Ulbrich 1983; Feingold and Levin 1986). Both surface disdrometers and aircraft imaging probes have been widely used to study the variability of the DSD especially as a function of the rain rate and to document the statistics of the DSD parameters. Such data are then used to develop algorithms based on radar observables, for example, Z–R relations or polarimetric radar algorithms for rain rate based on Z_h, Z_{dr}, and/or K_{dp}. The promise of dual-polarized radar has been the accurate retrieval of DSD parameters and rain rate using a physical basis as opposed to statistical/engineering approaches. For algorithm development, a physically based model of rain must be assumed with attention placed not only on the DSD model but also on the models for raindrop shape, material properties, and orientation. It has been customary to assume equilibrium oblate shapes (or, axis ratios) with slight adjustments to account for drop oscillations (Goddard and Cherry 1984; Andsager et al. 1999). The orientation of the drop's symmetry axis from a radar perspective is usually referred to as the canting angle (the angle between the projection of the symmetry axis on the polarization plane and the projection of the vertical direction on this same plane). Turbulence can cause a distribution of canting angles following a Gaussian model with zero mean and standard deviation $\lesssim 5°$ (Beard and Jameson 1983; Hendry et. al. 1987). Since both drop oscillations and

Corresponding author address: V. N. Bringi, Dept. of Electrical and Computer Engineering, Colorado State University, Fort Collins, CO 80523-1373.
E-mail: bringi@engr.colostate.edu

canting tend to bias the mean axis ratio slightly toward sphericity, Gorgucci et al. (2000, 2001, 2002) proposed the concept of an "effective" mean axis ratio versus diameter model, which is linear ($r = 1 - \beta_{eff} D$), and furthermore, they developed an algorithm for estimating $\hat{\beta}_{eff}$ from radar measurements of Z_h, Z_{dr}, and K_{dp}. A background section is included that provides more detail on the subject of drop oscillations/canting and the effective β concept.

In this paper, 2D video and RD-69 disdrometer DSD data are analyzed in a variety of climatic regimes from near equatorial to maritime to continental, and the variability of DSD parameters assuming a normalized gamma form is documented for comparison with polarimetric radar retrievals. The radar measurements used herein are samples from a variety of climatic regimes (Colorado, Florida, Brazil, and Kwajalein) obtained as part of the Tropical Rainfall Measurement Mission (TRMM) ground validation field programs. Data from the Colorado State University (CSU) CHILL, National Center for Atmospheric Research (NCAR) S-band polarimetric radar and the National Aeronautics and Space Administration (NASA) Kwajalein radars are analyzed for retrieval of the DSD parameters and rain rate, which are compared against disdrometer retrievals in a statistical manner.

2. Background

At low elevation angles and in the Rayleigh scattering limit, the radar observables Z_h (reflectivity at horizontal polarization), Z_{dr} (differential reflectivity), and K_{dp} (specific differential propagation phase) can be used to estimate the parameters of the raindrop size distribution subject to the assumption of a suitable model for raindrop size, shape and orientation distributions. The DSD is usually modeled as an exponential, gamma, or a lognormal form. Drop shapes are usually modeled as oblate spheroidal with axis ratio (ratio of minor to major axes, $r = b/a$) corresponding to equilibrium shapes that result from a balance between hydrostatic, surface tension, and aerodynamic forces (e.g., Green 1975; Beard and Chuang 1987). However, natural raindrops as well as drops simulated in a laboratory setting are known to exhibit steady-state oscillations as they fall. There are two preferred modes of the fundamental harmonic: (a) axisymmetric mode oscillations, which produce two-sided scatter in the axis ratio with respect to the equilibrium value; (b) transverse mode oscillations, which produce mostly one-sided scatter with respect to the equilibrium value; or (c) some combination of the two, termed as multimode oscillations (e.g., Beard 1984; Beard and Kubesh 1991; Andsager et al. 1999). Figure 1 illustrates a computer-generated oscillation sequence for a 5-mm drop showing the equilibrium shape (extreme lower-right panel), axisymmetric mode (shown in the two squares with light backgrounds), transverse mode (shown in the two squares with darkest back-

grounds) and multimode (four "gray" squares). Steady-state oscillations for drops $\lesssim 2$ mm in size are well understood, but oscillation amplitudes and modes for larger-sized drops are still uncertain. From a radar perspective, the horizontal and vertical polarization states are lined up along the major and minor axes of the equilibrium oblate shape (lower-right panel in Fig. 1). It follows that the equilibrium shape of the axisymmetric mode oscillations will present an oriented view to the radar with symmetry axis along the vertical polarization state. However, transverse or multimode oscillations will present an orientation distribution (or an effective canting angle distribution in the plane of polarization of the incident wave). Such an effective canting angle distribution is different from canting due to turbulence, which is modeled as Gaussian with zero mean and standard deviation typically $\lesssim 5°$ (Beard and Jameson 1983).

The slight shift in axis ratios from equilibrium values is provided by 2D video disdrometer analysis of artificial water drops imaged by a two-camera optical instrument after a fall distance of 35 m. A detailed description of this instrument is available in Kruger and Krajewski (2002). The fall distance of 35 m is sufficient that initial oscillations produced by the water hose (used in this study) should have decayed leaving only the steady-state oscillations to be captured by the disdrometer (see Fig. 3 of Andsager et al. 1999). The mean axis ratio versus equivalent spherical diameter for drops $\gtrsim 2$ mm is shown in Fig. 2 (along with $\pm 1\sigma$ standard deviation bars). These data are compared with the fit recommended by Andsager et. al. (1999) for $1 < D$ (equivalent diameter) < 4 mm, which accounts for transverse oscillations and the equilibrium axis ratio model of Beard and Chuang (1987) for $D < 1$ and $D > 4$ mm. Excellent agreement is noted between the fit and the data for $2 < D < 3.75$ mm. The water hose data show evidence of steady-state oscillations. There is a slight upward shift in mean axis ratio relative to the Beard–Chuang equilibrium model for all drops from 2–8 mm. A measure of the oscillation amplitude can be ascertained from the histogram of normalized axis ratio shown in Fig. 3 for the same dataset (normalized means that the measured axis ratio is divided by its mean for all drops within a specified equivalent diameter interval). The mode in Fig. 3 is very close to unity with standard deviation of 0.157. The two-sided scatter in Fig. 2 implies that the oscillation mode could not be pure transverse (which would exhibit one-sided scatter; Beard and Kubesh 1991). It also implies that there is a distribution of oscillation amplitudes with a relatively large fraction of drops experiencing low amplitudes (since the mode is very close to unity).

The implication of the water hose data for the rain model are as follows. The axis ratio distribution can be assumed to be symmetric about its mean with small variance. In addition, a linear relation between mean axis ratio ($\bar{r}$) and D can be assumed of the form $\bar{r} = 1 - \beta D$ where the slope β is variable to account for the
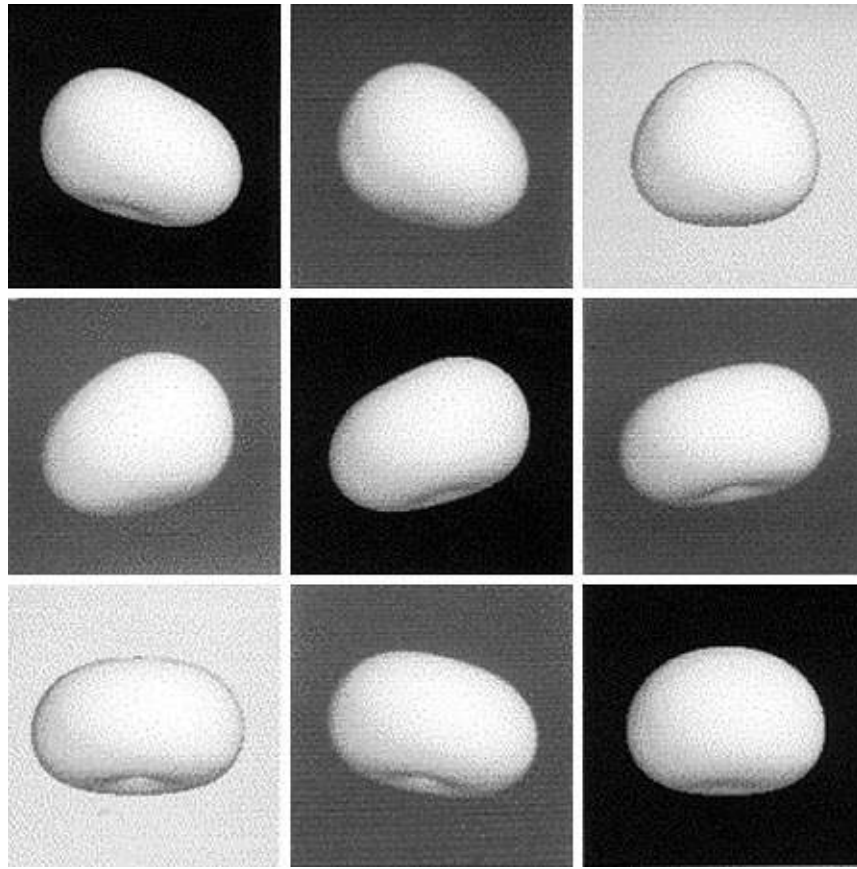
FIG. 1. Computer-generated oscillation sequence for a 5-mm drop: (bottom right) depiction of the static shape. The four ''gray'' squares show mixed mode oscillation (equal mixes of pure transverse mode in the two squares with the darkest backgrounds and pure vertical mode in the two squares with light backgrounds). The mixed mode shows an effective canting angle as seen by radar or 2D video disdrometer. (Courtesy of Prof. Ken Beard, University of Illinois.)
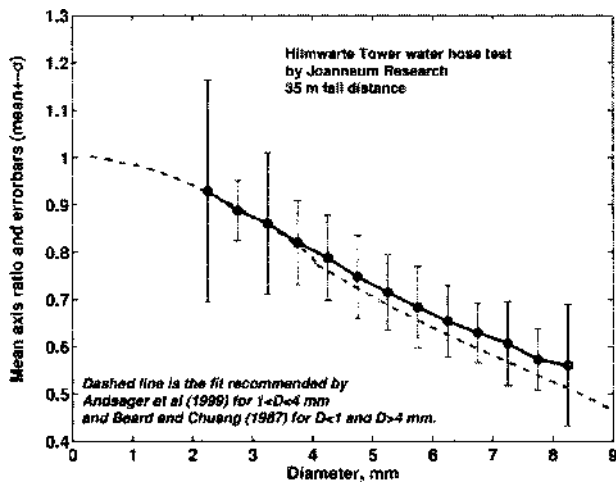

FIG. 2. Mean axis ratio and std dev bars vs D based on 2D video images of water drops from the water hose test.
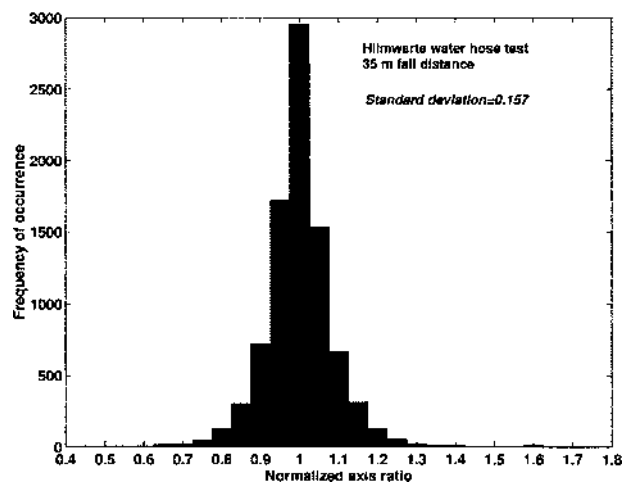

FIG. 3. Histogram of normalized axis ratio of drops with $D > 2$ mm from water hose test.

TABLE 1. Locations for disdrometer data and available number of 2-min averaged DSDs in convective (and stratiform) rain.

Location	No. of 2-min samples*	Type of disdrometer
Darwin, Australia	1074 (1528)	RD-69
SCSMEX	397 (688)	RD-69
Papua New Guinea	1018 (1623)	2D video
Florida	145 (273)	2D video
Colorado	54 (60)	2D video
TOGA COARE	From Testud et al. (2001)	Airborne particle measuring system probe
Arecibo, Puerto Rico	From Ulbrich et al. (1999)	RD-69
Graz, Austria	94 (1952)	2D video
Sydney, Australia	461 (4371)	RD-69
Kwajalein	— (690)	RD-69

* Stratiform rain samples are in parentheses. Convective rain samples are for $R \geq 5$ mm h^{-1} and std dev of R over five consecutive 2-min samples >1.5 mm h^{-1}.

effects of multimode oscillations in slightly shifting the mean axis ratio away from the equilibrium axis ratio. Since natural raindrops will be subject to both multimode oscillations as well as turbulence, a simple way to account for both effects is via an effective canting angle distribution that is Gaussian with mean of 0° and with unknown but larger standard deviation (σ_{eff}). Using such a model the specific differential phase (K_{dp}) at long wavelengths can be expressed as (Jameson 1985; Bringi and Chandrasekar 2001)

$$K_{\mathrm{dp}} = \left(\frac{180°}{\lambda}\right) 10^{-3} C W D_m \beta \, \exp(-2\sigma_{\mathrm{eff}}^2), \qquad (1)$$

where λ is the wavelength in meters, W is the rain water content in grams per cubic meter, D_m is the mass-weighted mean diameter in millimeters (defined later in section 3), C is a constant (≈ 3.75) and is dimensionless, β is the slope of the mean axis ratio versus D relation, and σ_{eff} is the effective standard deviation of the canting angle distribution. The product $\beta \exp(-2\sigma_{\mathrm{eff}}^2)$ may be defined as an effective slope parameter (β_{eff}), which can account for both multimode oscillations as well as canting. Even if the mean axis ratio versus D relation is nonlinear (e.g., Fig. 2), it is possible to define a linear relation ($\bar{r} = 1 - \beta_{\mathrm{eff}} D$) with β_{eff} adjusted such that it results in the same K_{dp} (for a given value of the product $W D_m$) as the nonlinear form. Gorgucci et al. (2000) recognized this concept of an effective slope parameter (simply termed the effective β concept), and proceeded to develop an algorithm to estimate $\hat{\beta}_{\mathrm{eff}}$ from radar measurements of Z_h, Z_{dr}, and K_{dp}.

There is mounting evidence that $\hat{\beta}_{\mathrm{eff}}$ is slightly smaller in maritime rain versus continental rain (Gorgucci et al. 2001; May et al. 1999; Bringi et al. 2001a). There is also indirect evidence from studies that compare rain accumulation using the $R(K_{\mathrm{dp}})$ estimator with gauge data. The $R(K_{\mathrm{dp}})$ algorithms developed so far have assumed equilibrium drop shapes and $\sigma_{\mathrm{eff}} \lesssim 5°$, so that they tend to generally underestimate the radar rainfall relative to gauge accumulations (May et al. 1999; Petersen et al. 1999; Ryzhkov and Zrnic 1996; Brandes et al. 2001) especially in maritime-like rain events or

in rainfall events dominated by small drops. For example, if the $R(K_{\mathrm{dp}})$ algorithm assumes a β_{eff} of 0.06 mm^{-1} whereas the actual β_{eff} is 0.05, the bias in rain rate would be around 30% (underestimate). The $R(K_{\mathrm{dp}}, \beta_{\mathrm{eff}})$ algorithm developed by Gorgucci et. al. (2000, 2001) will correct for this bias.

A similar situation exists for the estimation of the mass-weighted mean diameter (D_m) of the DSD using Z_{dr} (Goddard et al. 1982; Goddard and Cherry 1984). These latter references were the first to suggest that mean drop axis ratios should be adjusted slightly upward relative to equilibrium axis ratios based on comparisons between radar-measured Z_{dr} and D_m inferred from a disdrometer in light rainfall. More recently, Gorgucci et al. (2002) proposed algorithms for estimating D_m (or, the median volume diameter D_o defined in section 3) using β_{eff}, Z_h, and Z_{dr} and showed through simulation that the retrieval accuracy was in the range 4%–8% in the absence of any radar measurement errors (including such errors, the accuracy ranged from 5%–20%). Similarly, the normalized "intercept" parameter (N_w) of a gamma DSD (defined in section 3) can also be estimated from β_{eff}, Z_h, and Z_{dr}. The extension of the methodology to retrieval of D_m and N_w in cases where radar measured K_{dp} and/or Z_{dr} may be too "noisy" (such as in stratiform rain or low convective rain rates) was proposed and evaluated by Bringi et al. (2002). In this paper, the retrieval of D_m and N_w based on radar measurements of Z_h, Z_{dr}, and K_{dp}, and using the β_{eff} concept, are applied to radar data from a variety of climatic regimes such as Colorado, Florida, Brazil, and Kwajalein (central tropical Pacific).

3. Disdrometer data

Disdrometers (or, drop sizing meters) are used to measure the DSD at a given location and are useful in determining the statistical characteristics of the DSD. In this study data from the RD-69 (Joss and Waldvogel 1967) and 2D-video disdrometers in different climatic regimes are analyzed. Table 1 lists the geographical locations and the available number of 2-min averaged

samples of the DSD at each location for convective and stratiform rain types. A simple scheme is used to separate stratiform and convective rain types based on the standard deviation of rain rate over 5 consecutive DSD samples. If this standard deviation is ≤ 1.5 mm h^{-1} then it is classified as stratiform, otherwise it is assumed to be convective (this threshold is based on data acquired by the 2D video disdrometer in Colorado during a stratiform upslope event with radar-observed "brightband" signature).

For each 2-min averaged DSD sample, the mass-weighted mean diameter (D_m) is computed as the ratio of the 4th to 3rd moment of the DSD:

$$D_m = \frac{E[D^4]}{E[D^3]}, \quad (2)$$

where E stands for expectation. Also, the water content is calculated as

$$W = \frac{\pi}{6}\rho_w E[D^3], \quad (3)$$

where ρ_w is the water density. A generalized intercept parameter (N_w) is computed from W and D_m:

$$N_w = \frac{4^4}{\pi\rho_w}\left(\frac{W}{D_m^4}\right). \quad (4)$$

The N_w is the same as the parameter N_o of an equivalent exponential DSD (typically in units of mm^{-1} m^{-3}), which has the same W and D_m as the measured DSD:

$$N(D) = \frac{4^4}{\pi\rho_w}\left(\frac{W}{D_m^4}\right)\exp\left(-\frac{4D}{D_m}\right) \quad (5a)$$

$$= N_o \exp\left(-\frac{4D}{D_m}\right). \quad (5b)$$

One measure of the shape of the DSD is provided by the normalized standard deviation of the mass spectrum (σ_M) with respect to D_m (Ulbrich and Atlas 1998):

$$\frac{\sigma_M}{D_m} = \left\{\frac{E[D^3(D-D_m)^2]}{D_m^2 E(D^3)}\right\}^{1/2}. \quad (6)$$

Note that the parameters derived from the measured DSD are now N_w, D_m, and σ_M/D_m, which are estimated without any assumption about the form of the DSD, for example, gamma or lognormal (Testud et al. 2001). The median volume diameter (D_o) is often used instead of D_m (but is closely related to it) and is defined by

$$\frac{\pi}{6}\rho_w \int_0^{D_o} D^3 N(D)\, dD = \frac{1}{2}W. \quad (7)$$

The normalized gamma DSD is now defined based on (Sekhon and Srivastava 1971; Willis 1984; Testud et al. 2001),
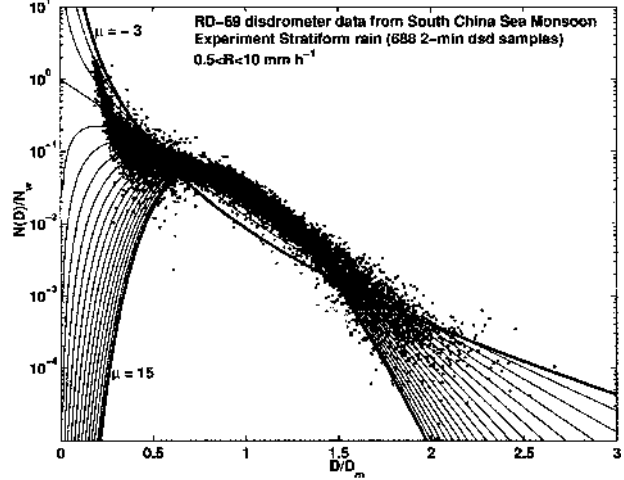

FIG. 4. The scaled DSD $N(D)/N_w$ vs the normalized diameter D/D_m for data from the RD-69 disdrometer acquired during the SCSMEX. Solid lines are the normalized gamma distribution for μ from -3 to 15 in steps of 1.

$$N(D) = N_w f(\mu)\left(\frac{D}{D_m}\right)^\mu \exp\left[-(4+\mu)\frac{D}{D_m}\right], \quad (8a)$$

where

$$f(\mu) = \frac{6}{4^4}\frac{(4+\mu)^{\mu+4}}{\Gamma(\mu+4)}. \quad (8b)$$

The parameter μ is a measure of the shape of the gamma DSD. The normalizing of drop diameter by D_m and scaling the $N(D)$ by N_w make it possible to compare DSDs with widely differing rain rates. For example, Fig. 4 shows $N(D)/N_w$ versus D/D_m from stratiform rain from the South China Sea Monsoon Experiment (SCSMEX) using an RD-69 disdrometer together with an overlay of the scaled gamma form $N(D)/N_w = f(\mu)x^\mu \exp[-(4 + \mu)x]$, where $x = D/D_m$. Note that the measured DSDs, when scaled/normalized in this manner, are well bounded by the family of scaled gamma functions as μ varies over the range -3 to 15. While there are several methods of normalizing/scaling the measured DSD (e.g., Sempere-Torres et al. 1994), the method used here is advantageous in several respects (Willis 1984; Illingworth and Blackman 1999). The dual-polarized radar observables Z_{dr} and K_{dp} are proportional to D_m, and the product WD_m, respectively, at long wavelengths. From the viewpoint of fitting the measured DSD with a gamma form, the optimal μ value may be numerically determined by minimizing the absolute deviation between the scaled/normalized DSD data and the scaled gamma form $f(\mu)x^\mu \exp[-(4 + \mu)x]$. Note from Fig. 4 that the scaled gamma form has two "pivot" points near $D/D_m \approx 0.75$ and $D/D_m \approx 1.5$, which make the μ estimation more robust as compared with other methods (e.g., moment methods; Ulbrich and Atlas 1998). Finally, the parameters N_w, D_m, and μ estimated using this proce-
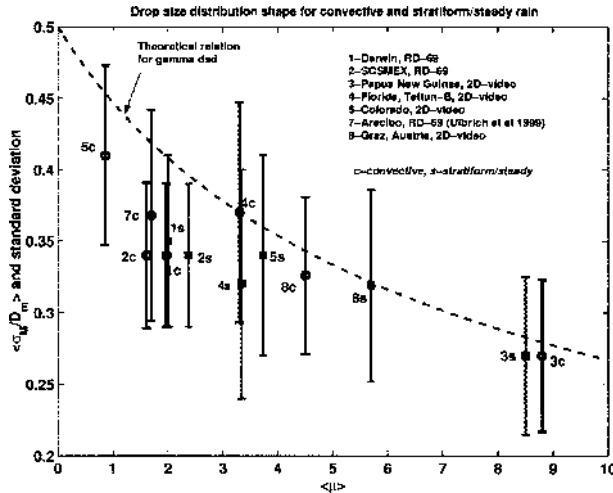
FIG. 5. The average value of σ_M/D_m (and $\pm1\sigma$ bars) vs average μ based on disdrometer data from different climatic regimes.

dure provide measures of concentration, mass-weighted mean diameter, and DSD shape, respectively.

The median volume diameter (D_o) is related to D_m for gamma DSD as

$$\frac{D_o}{D_m} = \frac{3.67 + \mu}{4 + \mu}, \tag{9}$$

and the σ_M/D_m is related to μ as

$$\frac{\sigma_M}{D_m} = \frac{1}{(4 + \mu)^{1/2}}. \tag{10}$$

The above relations and the effects of drop truncation on the estimation of μ, D_m, and N_o using the moment method are given in Ulbrich and Atlas (1998).

It is illustrative to see how closely the average shape of the measured DSD data follow the theoretical relation in (10), which is valid in the absence of any truncation effects. Figure 5 shows the average value of σ_M/D_m (with ±1 standard deviation in bars) versus average μ for the set of disdrometer data (listed in Table 1) from different climatic regimes. While the data points corresponding to 2D video disdrometer measurements tend to agree with the theoretical relation in (10) fairly well, the cluster of four data points near $\langle\mu\rangle = 2$ and $\langle\sigma_M/D_m\rangle = 0.35$ based on RD-69 disdrometer data are biased low relative to (10). While it is believed that the μ estimate here is robust with respect to drop truncation effects for the RD-69 (otherwise the $\langle\mu\rangle$ value would be very high), such is not the case with respect to the estimate of $\langle\sigma_M/D_m\rangle$, which is likely to be biased low, in accord with Fig. 5. Examination of Fig. 5 shows that on average, the DSD shape is quite different from exponential (for which $\mu = 0$). Extreme values of $\langle\mu\rangle \approx 9$ and low $\langle\sigma_M/D_m\rangle \approx 0.26$ are obtained in Papua New Guinea (close to the equatorial regime), while the Colorado convective rain data show $\langle\mu\rangle \approx 1$ and $\langle\sigma_M/D_m\rangle \approx 0.4$, which is more representative of the High Plains

regime of the United States. To summarize, Fig. 5 illustrates the fact that the average shape of the DSD can be represented by the gamma form based on the 2D video measurements with $\langle\mu\rangle$ ranging from 1 to around 10 for the available data from different climatic regimes.

As mentioned earlier, two disdrometers with very different measurement principles and measurement characteristics are used in this study. It is beyond the scope of this article to discuss the advantages/limitations of these instruments but, in general, the 2D video disdrometer is superior to the RD-69 except for small drop concentration estimates in very windy conditions. For a comparison of these two instruments see Williams et al. (2000) and Tokay et al. (2001), and references therein.

4. Radar analysis

The methodology for retrieval of N_w and D_o from radar measurements of Z_h, Z_{dr}, and K_{dp} is described in Bringi et al. (2001a) and applied there to one squall-line event from the TRMM Large-Scale Biosphere–Atmosphere Experiment in Amazonia (LBA) ground validation program. In this study, the same methodology is applied to retrieval of N_w and D_o from rain events from several different climatic regimes, in particular, Colorado, Florida, and Kwajalein.

The S-Pol radar operates at S band and uses a mechanical polarization switch and two separate receivers to measure the polarimetric covariance matrix (Randall et al. 1997). The CSU-CHILL radar uses two separate transmitters and two receivers to measure the covariance matrix (Brunkow et al. 2000). The Kwajex radar also operates at S band but uses the "hybrid" measurement scheme involving transmission of a polarization state with equal power in its horizontal and vertical components (with arbitrary phase). The horizontal and vertical polarized components of the received signal are routed into two separate receivers (e.g., Bringi and Chandrasekar 2001; Brunkow et al. 2000; Doviak et al. 2000). The radar data stream consists of Z_h, Z_{dr}, and Φ_{dp} (differential propagation phase), which are available every 150 m in range. The Φ_{dp} are filtered in range using the iterative method of Hubbert and Bringi (1995). The filtered Φ_{dp} range profiles are used to estimate K_{dp} based on the slope of a least-squares fit line. An adaptive technique is used for selecting the number of range samples used in the least-squares fit, that is, 30 samples if $Z_h \leq 35$ dBZ, 20 if $35 < Z_h \leq 45$ dBZ, and 10 for $Z_h > 45$ dBZ. The Z_h data are corrected for attenuation using the algorithm of Testud et al. (2000) adapted for S-band, while Z_{dr} is corrected for differential attenuation using a selfconsistent, constraint-based algorithm described by Bringi et al. (2001b). These corrections are significant only when the total Φ_{dp} exceeds around 50°. The corrected Z_h and Z_{dr} data are then averaged in range using uniform block averaging for the different Z_h ranges used earlier for K_{dp} estimation. The effective β is
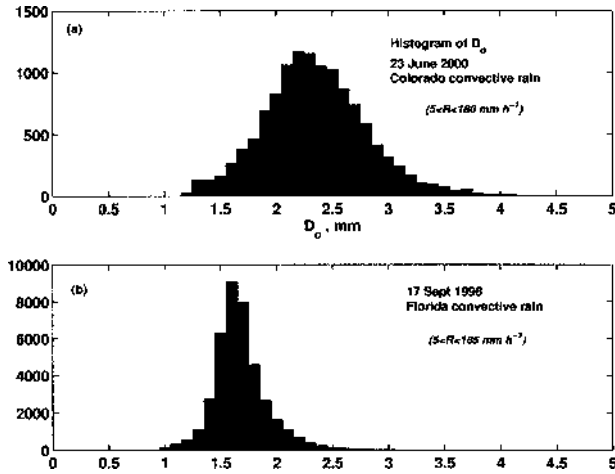
FIG. 6. Histogram of D_o retrieved from S-Pol radar data: (a) 23 Jun 2000 event in Colorado; (b) 17 Sep 1998 event in Florida.
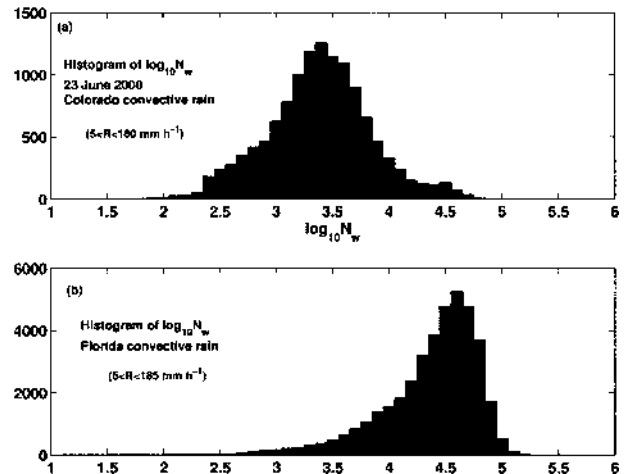

FIG. 7. As in Fig. 6, except histogram of $\log_{10}N_w$ (units of N_w in mm^{-1} m^{-3}).

computed based on the averaged Z_h, Z_{dr}, and K_{dp} data and $D_o(\beta_{eff}, Z_h, Z_{dr})$; $N_w(\beta_{eff}, Z_h, Z_{dr})$; and $R(\beta_{eff}, Z_h, Z_{dr})$ are calculated using algorithms developed by Gorgucci et al. (2001, 2002), which are summarized in Bringi et al. (2002; see appendix). Because the β_{eff} can only be computed in moderate to high rain rates, the thresholds used here are $Z_h \geq 35$ dBZ, $Z_{dr} \geq 0.2$ dB, and $K_{dp} \geq 0.3° $ km^{-1}. When Z_h is arbitrary and $Z_{dr} \geq 0.2$ dB but K_{dp} is too noisy, the D_o, N_w, and R retrievals are essentially based on a constant value of β_{eff} (in the range 0.045–0.0475 mm^{-1}) together with the measured Z_h and Z_{dr}. When $Z_h < 35$ dBZ and $Z_{dr} < 0.2$ dB, an indirect method is used to estimate D_o as explained in Bringi et al. (2002). Briefly, the hypothesis is that even though Z_{dr} data are noisy at low Z_h and tend on average to near 0 dB at very light rain rates, scattering simulations based on disdrometer DSD samples (and assuming a constant β_{eff} in the range given earlier) show that the mean relation between Z_{dr} and Z_h should be a power law with fixed exponent of the form $Z_{dr} = \alpha Z_h^{0.28}(Z_{dr}$ in dB; Z_h in mm^6 m^{-3}). The multiplicative coefficient α is estimated from the data (with $0 \leq Z_h \leq 35$ dBZ) as $\hat{\alpha} = \langle Z_{dr}\rangle/\langle Z_h^{0.28}\rangle$, where angle brackets denote average value. The retrieval of D_o and N_w follow essentially assuming β_{eff} is constant together with measured Z_h and Z_{dr} inferred from the power-law fit. One caveat in using this methodology is that the accuracy of Z_h and Z_{dr} should be high (typically to within ± 1 dBZ for Z_h and to within ± 0.1 dB for Z_{dr}, or better).

The radar retrievals of D_o and N_w were generally based on data acquired from a single storm event in each location. A preselected polar area was identified as convective or stratiform rain based on radar characteristics and data were accumulated over a period of 5 min or so. The stratiform rain in nearly all cases corresponded to the trailing stratiform area of a convective squall line–like event. Convective rain areas generally corresponded to rain cells in a squall line or

multicellular-type storm events. Typically, the N_w and D_o values could be retrieved from tens of thousands of range resolution volumes within a few minutes covering a wide range of rain rates. The large spatial sampling by radar generally ensures that a range of DSDs have been sampled.

Figure 6 shows histograms of D_o in convective rain retrieved using S-Pol radar data from one event in Colorado and one in Florida. Note how much broader the D_o histogram is with mode near 2.3 mm for the Colorado case, reflecting the microphysics of rain formation in the High Plains via the melting of graupel and tiny hailstones. In contrast, the Florida event has a much narrower distribution of D_o with significantly smaller modal value of $D_o \approx 1.6$ mm even though the span of radar-derived rain rates in both events is nearly the same. This reflects warm rain microphysics and evolution of the DSD within a much deeper layer from the melting level to the surface in Florida ($\sim$4 km) as compared to Colorado ($\sim$2 km). Figure 7 shows the histogram of $\log_{10}(N_w)$ from Colorado and Florida. Note that the units of N_w are in mm^{-1} m^{-3} (the Marshall–Palmer value of $N_w = 8000$ or $\log N_w = 3.9$). The Colorado histogram is nearly symmetric about the modal value of $N_w \approx$; 2500 mm^{-1} m^{-3}, whereas the Florida histogram is quite skewed with modal value of $N_w \approx 40\,000$ mm^{-1} m^{-3}. On average, the DSD characteristics conform to the qualitative view that convective rain in Colorado consists of a lower concentration of relatively larger-sized drops whereas the opposite is true in Florida. It also follows that for a given reflectivity, the convective rain rate in Colorado will be much less than in Florida [around a factor 2.5 less, based on $Z \propto N_w^{-0.5} R^{1.5}$ and using the modal N_w values; Testud et al. (2001)]. In other words, the multiplicative coefficient in the $Z = aR^{1.5}$ power-law relation will be a factor 2.5 higher in Colorado as compared to Florida in general agreement with numerous disdrometer-based studies comparing Z–
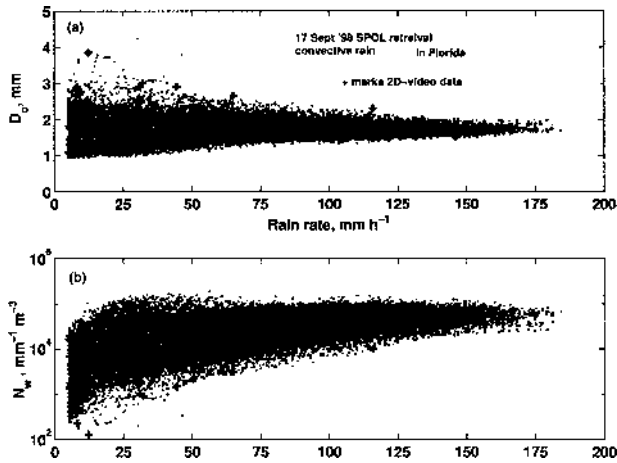
FIG. 8. (a) Median volume diameter D_o vs R for convective rain on 17 Sep 1998 retrieved from S-Pol radar measurements (gray dots). The "+" marks 2D video data from Florida acquired during the TEFLUN-B project. (b) As in (a), except N_w vs R for convective rain.

R relations from the Tropics to the continental (e.g., Ulbrich 1983).

Figure 8 shows D_o and N_w versus R for the Florida convective event as retrieved from S-Pol radar measurements. Also overlaid on this figure are data points obtained from analysis of 2D video disdrometer measurements in convective rain during the TRMM Texas Florida Underflights (TEFLUN-B) program. It should be emphasized that the radar retrievals are based on a single convective event but the spatial sampling by the radar of convective rain cells in different stages of their life cycle tends to capture a wide range of DSD variability, significantly more than what a single disdrometer at a fixed location can capture over several months. Figure 8 shows that the radar retrievals are not only reasonable when compared to 2D video disdrometer data but, in addition, very few disdrometer data points lie outside the radar derived "envelope" of D_o and N_w. At high rain rates, the radar and disdrometer D_o values tend to a stable value around 1.7–2.0 mm, reflecting the tendency to equilibrium-like distributions where drop breakup and coalescence are in near balance (e.g., Hu and Srivastava 1995). Under equilibrium condition, D_o is constant and any increase in rain rate is due to an increase in N_w.

Figure 9 shows similar results except for stratiform rain in Florida. Again, the radar retrieval is based on a single event but the large areal sampling results in a large number of data points. The stratiform area was selected based on radar RHI observations, which showed a brightband signature. Also overlaid on Fig. 9 are 2D video disdrometer data points from stratiform rain during the TEFLUN-B program. Generally, the radar retrieval captures the DSD variability quite well, and again only a few disdrometer data points lie outside the envelope established by the radar retrieval. This feature also holds for radar retrievals in convective and
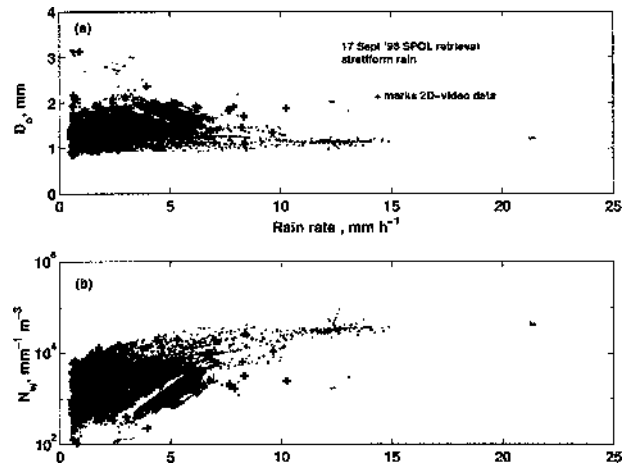

FIG. 9. As in Fig. 8, except data from stratiform rain.

stratiform rain during other field programs (TRMM LBA, Colorado, and Kwajalein) but are not shown here.

5. Composite statistics from radar and disdrometer data

One way of showing the statistics of N_w and D_o from different climatic regimes is to plot $\log_{10}\langle N_w\rangle$ versus $\langle D_o\rangle$, where angle brackets denote an average value. It is also illustrative to plot the $\pm 1\sigma$ standard deviation bars around $\log_{10}\langle N_w\rangle$. Figure 10 shows the composite results based on disdrometer data (see Table 1) and from radar retrievals (events are marked on the figure) for stratiform rain, while Fig. 11 shows the same for convective rain. Note that $\langle D_m\rangle$ is plotted here rather than $\langle D_o\rangle$. The radar-derived $\langle D_o\rangle$ is translated to $\langle D_m\rangle$ using (9) with $\langle\mu\rangle$ obtained from disdrometer data for the
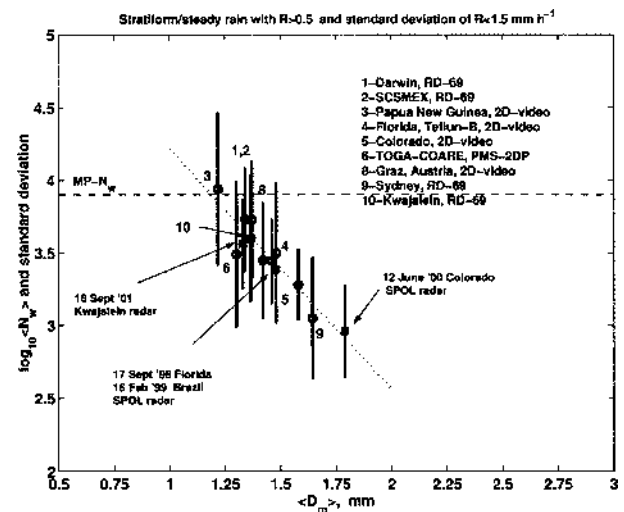

FIG. 10. The average value of $\log_{10}N_w$ (with $\pm 1\sigma$ std dev bars) vs average D_m from disdrometer data and radar retrievals as indicated for stratiform rain. Dotted straight line is the least squares fit.
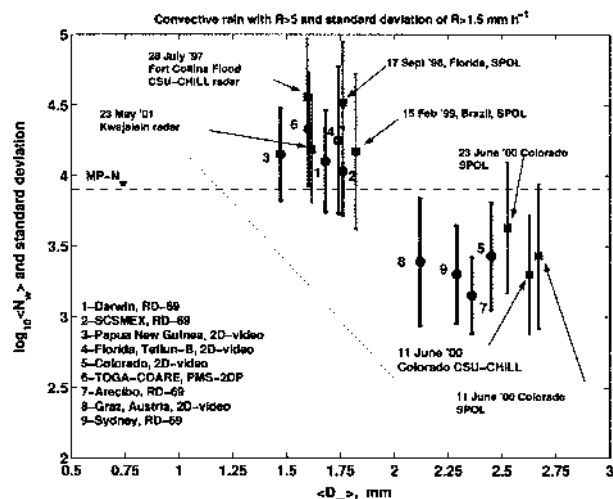
FIG. 11. As in Fig. 10, except for convective rain. Dotted line is
the fit to stratiform rain in Fig. 10.

various climatic regimes in question (Colorado, Brazil, Kwajalein, and Florida); the adjustment from $\langle D_o \rangle$ to $\langle D_m \rangle$ is slight and in the range 4%–7% but necessary for comparison with the disdrometer estimates of $\langle D_m \rangle$.

Figure 10 for stratiform rain clearly shows that there is an inverse relationship between $\log_{10}\langle N_w \rangle$ and $\langle D_m \rangle$; in fact, it is quite remarkable that a straight line fit (shown as a dashed line) results from the composite disdrometer/radar retrievals that encompass a number of climatic regimes from near the equator (Papua New Guinea, marked as 3) to the High Plains (Colorado, marked as 12 June 2000 event). From a microphysical perspective, stratiform rain results via the melting of snowflakes and/or tiny graupel or rimed particles. If the bright band is "strong," then it likely reflects melting of larger, low-density and dry snowflakes into rain, whereas if the bright band is "weak" then it may reflect the melting of tiny, compact graupel or rimed snow particles (Fabry and Zawadzki 1995; Waldvogel et al. 1995). In fact, the transition from large, dry snowflakes to tiny, compact graupel or rimed particles during a stratiform rain event leads to the so-called N_o-jump effect (Waldvogel 1974). In essence, the large, low-density snowflakes lead to DSDs that have smaller $\langle N_w \rangle$ and larger $\langle D_m \rangle$ relative to the tiny, compact graupel or rimed snow particles. The straight line in Fig. 10 may reflect such microphysical differences in stratiform rain DSDs from different climatic regimes.

Figure 11 shows similar results for convective rain. There appears to be a cluster of data points with $\langle D_m \rangle \approx$ 1.5–1.75 mm and $\log_{10}\langle N_w \rangle \approx$ 4–4.5, the regime varying from near the equator (Papua New Guinea) to subtropics (Florida, Brazil) to oceanic [Tropical Ocean Global Atmosphere Coupled Ocean–Atmosphere Response Experiment (TOGA COARE), Kwajalein, SCSMEX]. This cluster may be referred to as a "maritime-like" cluster where rain DSDs are characterized

by a higher concentration of smaller-sized drops. The Fort Collins flash flood event is unusual for Colorado as the data fall in the maritime-like cluster (this was confirmed independently by Petersen et al. 1999). The second "cluster" is characterized by $\langle D_m \rangle \approx$ 2–2.75 mm and $\log_{10}\langle N_w \rangle \approx$ 3–3.5, the regime varying from the U.S. High Plains (Colorado) to continental (Graz, Austria) to subtropics (Sydney, Australia) to Tropics (Arecibo, Puerto Rico). The Arecibo RD-69 disdrometer data was analyzed by Ulbrich et al. (1999) and reflects the average of seven thunderstorm events. They also note that the Arecibo thunderstorm rain DSDs are similar to continental thunderstorm rain and not at all similar to oceanic thunderstorm rain, which is in agreement with Fig. 11. Perhaps a similar situation is valid for the Sydney data. It is interesting to note that orographic effects may be prevalent in both Arecibo and Sydney. The "continental-like" cluster may be defined as that which reflects rain DSDs characterized by a lower concentration of larger-sized drops as compared with the previously-defined maritime-like cluster.

6. Summary and conclusions

The promise of dual-polarized radar in retrieving the two important parameters of the raindrop size distribution—that is, D_o and N_w—has, in our opinion, been generally achieved. It is implicit that such retrievals are representative of the spatial scale of radar measurements (typically several kilometers in range and 1° in cross-beam direction). An important advance has been the effective β concept, which accounts for the effects of drop oscillations and canting. Indeed, the rain model, which is assumed to have a gamma DSD form has been extended to include the effects of drop oscillation and canting via the β_{eff} parameter. Previously developed algorithms for estimating β_{eff}, and then in turn estimating $D_o(\beta_{eff}, Z_h, Z_{dr})$ and $N_w(\beta_{eff}, Z_h, Z_{dr})$ have been applied to radar retrievals in different climatic regimes such as Colorado, Brazil, Florida, and Kwajalein. The retrieval technique has also been previously extended to stratiform rain and to convective rain in those cases where the K_{dp} measurement is too noisy. The composite algorithms for D_o and N_w based on the triplet (Z_h, Z_{dr}, K_{dp}) or the couplet (Z_h, Z_{dr}) or simply on Z_h, depending on the reliability of the corresponding radar measurements, appear to be robust and in general agreement with disdrometer measurements for a wide range of rain rates. The same composite algorithm was used for radar data from Colorado, Brazil, Florida, and the NASA Kwajalein radar data from Kwajalein. One caveat is that the accuracy of Z_h and Z_{dr} measurements should be high (typically, ± 1 dB for Z_h and ± 0.1 dB for Z_{dr}, or better) and such accuracy is generally available in research quality radars.

DSD data from two different types of disdrometers (2D video and RD-69) have been analyzed to determine the variability of $\langle N_w \rangle$ and $\langle D_o \rangle$ in stratiform and con-

vective rain in different climatic regimes. The radar-retrieved values from Colorado, Brazil, Florida, and Kwajalein are in good agreement with disdrometer-derived values from the same or similar climatic regime. For stratiform rain, $\log_{10}\langle N_w\rangle$ and $\langle D_o\rangle$ are nearly linearly related with negative slope. These data appear to be consistent with microphysical differences in the formation of stratiform rain, for example, due to melting of large dry snowflakes (larger $\langle D_o\rangle$ and smaller $\langle N_w\rangle$) versus melting of smaller rimed ice particles (smaller $\langle D_o\rangle$ and larger $\langle N_w\rangle$). In the case of convective rain, a maritime-like cluster around $\langle D_o\rangle = 1.5$–1.75 mm and $\log_{10}\langle N_w\rangle = 4$–$4.5$ could be identified. A second cluster with $\langle D_o\rangle = 2$–2.75 mm and $\log_{10}\langle N_w\rangle = 3$–$3.5$ termed continental-like could also be identified. The change in $\langle N_w\rangle$ between these two clusters can be related to the well-known fact that the multiplicative coefficient in the $Z = aR^{1.5}$ relation is smaller in maritime rain than in continental rain ($a \propto N_w^{-0.5}$).

The behavior of D_o and N_w versus rain rate from the radar retrievals are generally consistent with disdrometer measurements. In particular, at high convective rain rates, the D_o tends to a constant value reflecting equilibrium-like DSD. There was only weak correlation between D_o and R (or, N_w and R) based on the radar retrievals as well as the disdrometer data. Finally, the average shape of DSDs from 2D video disdrometer data from several climatic regimes strongly suggests that the gamma form is a useful and applicable model. While a radar algorithm exists for estimating the gamma DSD shape parameter (μ), its validation is difficult and a subject of future research.

APPENDIX

Radar Retrieval of DSD Parameters

The method of retrieving D_o, N_w, and μ from Z_h, Z_{dr}, and K_{dp} is summarized here from Gorgucci et al. (2001, 2002). A gamma DSD model is assumed with the following ranges for the parameters:

$$0.5 \leq D_o \leq 3.5 \text{ mm} \tag{A1}$$

$$3 \leq \log_{10}N_w \leq 5, \quad \text{and} \tag{A2}$$

$$-1 < \mu \leq 5, \tag{A3}$$

with the additional constraint that $R < 300$ mm h^{-1} and $Z_h \lesssim 55$ dBZ. The parameters D_o, $\log_{10}N_w$, and μ are varied uniformly over their respective ranges to form a large table of D_o, N_w, and μ. Scattering calculations are performed at 2.8 GHz over a range of β_{eff}($0.02 \lesssim \beta_{eff} \lesssim 0.1$ mm^{-1}), and nonlinear regression is used to develop an algorithm for β (henceforth, the subscript "eff" will be dropped) in terms of Z_h, Z_{dr}, and K_{dp}:

$$\beta = 2.08Z_h^{-0.365} K_{dp}^{0.38} \xi_{dr}^{0.965} \text{ mm}^{-1}, \tag{A4}$$

where Z_h is in mm^6 m^{-3}, K_{dp} in degrees per kilometer, and ξ_{dr} is the differential reflectivity expressed as a ratio ($Z_{dr} = 10 \log_{10}\xi_{dr}$).

Simulations using gamma fits to measured drop size distributions (see section 3) and scattering calculations at 2.8 GHz of Z_h, Z_{dr}, and K_{dp} assuming, (i) mean axis ratio versus D fit of Andsager et al. (1999) for $1 \leq D \leq 4$ mm, and Beard and Chuang (1987) for $D < 1$ and $D > 4$ mm; (ii) Gaussian canting angle distribution with mean 0° and $\sigma = 10°$; and (iii) size integration up to $D_{max} = 2.5D_m$, show that β_{model} using (A4) is generally clustered around 0.045–0.0475 mm^{-1}, but is a nonlinear function of D_o (or equivalently ξ_{dr}). A nonlinear fit to the simulations yields

$$\beta_{model} = 0.0049(\xi_{dr})^2 - 0.0043(\xi_{dr}) + 0.0433;$$

$$\xi_{dr} > 1. \tag{A5}$$

The median volume diameter is then derived as

$$D_o = aZ_h^b(\xi_{dr})^c \text{ mm}^{-1}, \tag{A6}$$

where

$$a = 0.56, \tag{A7}$$

$$b = 0.064, \quad \text{and} \tag{A8}$$

$$c = 0.024\beta^{-1.42}. \tag{A9}$$

The N_w in units of mm^{-1} m^{-3} is derived as

$$\log_{10}N_w = aZ_h^b(\xi_{dr})^c, \tag{A10}$$

where now

$$a = 3.29, \tag{A11}$$

$$b = 0.058, \quad \text{and} \tag{A12}$$

$$c = -0.023\beta^{-1.389}. \tag{A13}$$

Parameter μ is derived as

$$\mu = \frac{aD_o^b}{\xi_{dr} - 1} - c(\xi_{dr})^d, \tag{A14}$$

where

$$a = 200\beta^{1.89}, \tag{A15}$$

$$b = 2.23\beta^{0.039}, \tag{A16}$$

$$c = 3.16\beta^{-0.046}, \quad \text{and} \tag{A17}$$

$$d = 0.374\beta^{-0.355} \text{ mm h}^{-1}, \tag{A18}$$

The rain rate is derived as

$$R = 0.105\beta^{0.865}Z_h^{0.93}(\xi_{dr})^c, \tag{A19}$$

where

$$c = -0.585\beta^{-0.703}. \tag{A20}$$

In this paper, the thresholds used are $Z_h \geq 35$ dBZ, $Z_{dr} \geq 0.2$ dB, and $K_{dp} \geq 0.3°$ km^{-1} for retrieval of D_o, N_w, m, and R using the above algorithms.

REFERENCES

Andsager, K., K. V. Beard, and N. F. Laird, 1999: Laboratory measurements of axis ratios for large raindrops. *J. Atmos. Sci.,* **56,** 2673–2683.

Beard, K. V., 1984: Oscillation modes for predicting raindrop axis and backscatter ratios. *Radio Sci.,* **19,** 67–74.

——, and A. R. Jameson, 1983: Raindrop canting. *J. Atmos. Sci.,* **40,** 448–454.

——, and C. Chuang, 1987: A new model for the equilibrium shape of raindrops. *J. Atmos. Sci.,* **44,** 1509–1524.

——, and R. J. Kubesh, 1991: Laboratory measurements of small raindrop distortion. Part II: Oscillation frequencies and modes. *J. Atmos. Sci.,* **48,** 2245–2264.

Brandes, E. A., A. V. Ryzhkov, and D. S. Zrnić, 2001: An evaluation of radar rainfall estimates from specific differential phase. *J. Atmos. Oceanic Technol.,* **18,** 363–375.

Bringi, V. N., and V. Chandrasekar, 2001: *Polarimetric Doppler Weather Radar: Principles and Applications.* Cambridge University Press, 636 pp.

——, G. Huang, V. Chandrasekar, and T. D. Keenan, 2001a: An areal rainfall estimator using differential propagation phase: Evaluation using a C-band radar and a dense gauge network in the Tropics. *J. Atmos. Oceanic Technol.,* **18,** 1810–1818.

——, T. D. Keenan, and V. Chandrasekar, 2001b: Correcting C-band radar reflectivity and differential reflectivity data for rain attenuation: A self-consistent method with constraints. *Trans. IEEE Geosci. Remote Sens.,* **39,** 1906–1915.

——, G. J. Huang, V. Chandrasekar, and E. Gorgucci, 2002: A methodology for estimating the parameters of a gamma raindrop size distribution model from polarimetric radar data: Application to a squall-line event from the TRMM/Brazil campaign. *J. Atmos. Oceanic Technol.,* **19,** 633–655.

Brunkow, D., V. N. Bringi, P. C. Kennedy, S. A. Rutledge, V. Chandrasekar, E. A. Mueller, and R. K. Bowie, 2000: A description of the CSU–CHILL National Radar Facility. *J. Atmos. Oceanic Technol.,* **17,** 1596–1608.

Doviak, R. J., V. N. Bringi, A. Ryzhkov, A. Zahrai, and D. S. Zrnić, 2000: Polarimetric upgrades to operational WSR-88D radars. *J. Atmos. Oceanic Technol.,* **17,** 257–278.

Fabry, F., and I. Zawadzki, 1995: Long-term radar observations of the melting layer of precipitation and their interpretation. *J. Atmos. Sci.,* **52,** 838–851.

Feingold, G., and Z. Levin, 1986: The lognormal fit to raindrop spectra from frontal convective clouds in Israel. *J. Climate Appl. Meteor.,* **25,** 1346–1364.

Goddard, J. W. F., and S. M. Cherry, 1984: The ability of dual-polarization radar (copolar linear) to predict rainfall rate and microwave attenuation. *Radio Sci.,* **19,** 201–208.

——, S. M. Cherry, and V. N. Bringi, 1982: Comparison of dual-polarization measurements of rain with ground-based disdrometer measurements. *J. Appl. Meteor.,* **21,** 252–256.

Gorgucci, E., G. Scarchilli, V. Chandrasekar, and V. N. Bringi, 2000: Measurement of mean raindrop shape from polarimetric radar observations. *J. Atmos. Sci.,* **57,** 3406–3413.

——, ——, ——, and ——, 2001: Rainfall estimation from polarimetric radar measurements: Composite algorithms independent of raindrop shape-size relation. *J. Atmos. Oceanic Technol.,* **18,** 1773–1786.

——, V. Chandrasekar, V. N. Bringi, and G. Scarchilli, 2002: Estimation of raindrop size distribution parameters from polarimetric radar measurements. *J. Atmos. Sci.,* **59,** 2373–2384.

Green, A. W., 1975: An approximation for the shape of large raindrops. *J. Appl. Meteor.,* **14,** 1578–1583.

Hendry, A., Y. M. M. Antar, and G. C. McCormick, 1987: On the relationship between the degree of preferred orientation in precipitation and dual polarization radar echo characteristics. *Radio Sci.,* **22,** 37–50.

Hu, Z., and R. C. Srivastava, 1995: Evolution of raindrop size distribution by coalescence, breakup and evaporation: Theory and observations. *J. Atmos. Sci.,* **52,** 1781–1783.

Hubbert, J., and V. N. Bringi, 1995: An iterative filtering technique for the analysis of copolar differential phase and dual-frequency radar measurements. *J. Atmos. Oceanic Technol.,* **12,** 643–648.

Illingworth, A. J., and T. M. Blackman, 1999: The need to normalize rsds based on gamma rsd formulations and implications for interpreting polarimetric radar data. Preprints, *29th Conf. on Radar Meteorology,* Montreal, QC, Canada, Amer. Meteor. Soc., 629–631.

Jameson, A. R., 1985: Microphysical interpretation of multi-parameter radar measurements in rain. Part III: Interpretation and measurement of propagation differential phase shift between orthogonal linear polarizations. *J. Atmos. Sci.,* **42,** 607–614.

Joss, J., and A. Waldvogel, 1967: A raindrop spectrograph with automatic analysis. *Pure Appl. Geophys.,* **68,** 240–246.

Kruger, A., and W. F. Krajewski, 2002: Two-dimensional video disdrometer: A description. *J. Atmos. Oceanic Technol.,* **19,** 602–617.

May, P. T., T. D. Keenan, D. S. Zrnić, L. D. Carey, and S. A. Rutledge, 1999: Polarimetric radar measurements of maritime rain at a 5-cm wavelength. *J. Appl. Meteor.,* **38,** 750–765.

Petersen, W. A., and Coauthors, 1999: Mesoscale and radar observations of the Fort Collins flash flood of 28 July 1997. *Bull. Amer. Meteor. Soc.,* **80,** 191–216.

Randall, M., J. Lutz, and J. Fox, 1997: S-POL's high isolation mechanical polarization switch. Preprints, *28th Conf. on Radar Meteorology,* Austin, TX, Amer. Meteor. Soc., 252–253.

Ryzhkov, A. V., and D. S. Zrnić, 1996: Assessment of rainfall measurement that uses specific differential phase. *J. Appl. Meteor.,* **35,** 2080–2090.

Sekhon, R. S., and R. C. Srivastava, 1971: Doppler radar observations of drop size distributions in a thunderstorm. *J. Atmos. Sci.,* **28,** 983–994.

Seliga, T. A., and V. N. Bringi, 1976: Potential use of radar differential reflectivity measurements at orthogonal polarizations for measuring precipitation. *J. Appl. Meteor.,* **15,** 69–76.

——, and ——, 1978: Differential reflectivity and differential phase shift: Applications in radar meteorology. *Radio Sci.,* **13,** 271–275.

Sempere-Torres, D., J. M. Porra, and J. D. Creutin, 1994: A general formulation for rain drop size distribution. *J. Appl. Meteor.,* **33,** 1494–1502.

Testud, J., E. Le Bouar, E. Obligis, and M. Ali-Mehenni, 2000: The rain profiling algorithm applied to polarimetric weather radar. *J. Atmos. Oceanic Technol.,* **17,** 322–356.

——, S. Oury, P. Amayenc, and R. A. Black, 2001: The concept of "normalized" distributions to describe raindrop spectra: A tool for cloud physics and cloud remote sensing. *J. Appl. Meteor.,* **40,** 1118–1140.

Tokay, A., A. Kruger, and W. F. Krajewski, 2001: Comparison of

drop size distribution measurements by impact and optical disdrometers. *J. Appl. Meteor.,* **40,** 2083–2097.

Ulbrich, C. W., 1983: Natural variations in the analytical form of the raindrop size distribution. *J. Climate Appl. Meteor.,* **22,** 1764–1775.

——, and D. Atlas, 1998: Rainfall microphysics and radar properties: Analysis methods for drop size spectra. *J. Appl. Meteor.,* **37,** 912–923.

——, M. Petitididier, and E. F. Campos, 1999: Radar properties of maritime rain found from disdrometer data at Arecibo, Puerto Rico. Preprints, *29th Int. Conf. on Radar Meteorology,* Montreal, QC, Canada, Amer. Meteor. Soc., 676–679.

Waldvogel, A., 1974: The N_o jump of raindrop spectra. *J. Atmos. Sci.,* **31,** 1067–1078.

——, H. Werner, and W. Schmid, 1995: Raindrop size distributions and radar reflectivity profiles. Preprints, *27th Int. Conf. on Radar Meteorology,* Vail, CO, Amer. Meteor. Soc., 26–30.

Williams, C. R., A. Kruger, K. S. Gage, A. Tokay, R. Cifelli, W. F. Krajewski, and C. Kummerow, 2000: Comparison of simultaneous raindrop size distributions estimated from two surface disdrometers and a UHF profiler. *Geophys. Res. Lett.,* **27,** 1763–1766.

Willis, P. T., 1984: Functional fits to some observed drop size distributions and parameterization of rain. *J. Atmos. Sci.,* **41,** 1648–1661.